Title

Revealing How Alkali Cations Affect the Surface Reactivity of Stainless Steel in Alkaline Aqueous Environments

Journal

ACS Omega, 3(11)

ISSN

2470-1343

Authors

Giron, Rachel Guia P
Chen, Xin
La Plante, Erika Callagon
et al.

Publication Date

2018-11-30

DOI

10.1021/acsomega.8b02227

Peer reviewed

ACS OMEGA

Article

Cite This: ACS Omega 2018, 3, 14680−14688

http://pubs.acs.org/journal/acsodf

Revealing How Alkali Cations Affect the Surface Reactivity of Stainless Steel in Alkaline Aqueous Environments

Rachel Guia P. Giron,[†] Xin Chen,[†] Erika Callagon La Plante,[†] Maxim N. Gussev,[‡] Keith J. Leonard,[‡] and Gaurav Sant*[,†,§,∥]

[†]Laboratory for the Chemistry of Construction Materials (LC^2), Department of Civil and Environmental Engineering, University of California, Los Angeles, 420 Westwood Plaza, Los Angeles, California 90095, United States

[‡]Materials Science and Technology Division, Oak Ridge National Laboratory, 1 Bethel Valley Road, Oak Ridge, Tennessee 37831, United States

[§]Department of Materials Science and Engineering, University of California, Los Angeles, 410 Westwood Plaza, Los Angeles, California 90095, United States

[∥]California NanoSystems Institute, University of California, Los Angeles, 570 Westwood Plaza, Los Angeles, California 90095, United States

ABSTRACT: Stainless steel is a ubiquitous structural material and one that finds extensive use in core-internal components in nuclear power plants. Stainless steel features superior corrosion resistance (e.g., as compared to ordinary steel) due to the formation of passivating iron and/or chromium oxides on its surfaces. However, the breakdown of such passivating oxide films, e.g., due to localized deformation and slip line formation following exposure to radiation, or aggressive ions renders stainless steel susceptible to corrosion-related degradation. Herein, the effects of alkali cations (i.e., K^+, Li^+) and the interactions between the passivated steel surface and the solution are examined using 304L stainless steel. Scanning electrochemical microscopy and atomic force microscopy are used to examine the inert-to-reactive transition of the steel surface both in the native state and in the presence of applied potentials. Careful analysis of interaction forces, in solution, within ≤10 nm of the steel surface, reveals that the interaction between the hydrated alkali cations and the substrate affects the structure of the electrical double layer (EDL). As a result, a higher surface reactivity is indicated in the presence of Li^+ relative to K^+ due to the effects of the former species in disrupting the EDL. These findings provide new insights into the role of the water chemistry not only on affecting metallic corrosion but also in other applications, such as batteries and electrochemical devices.

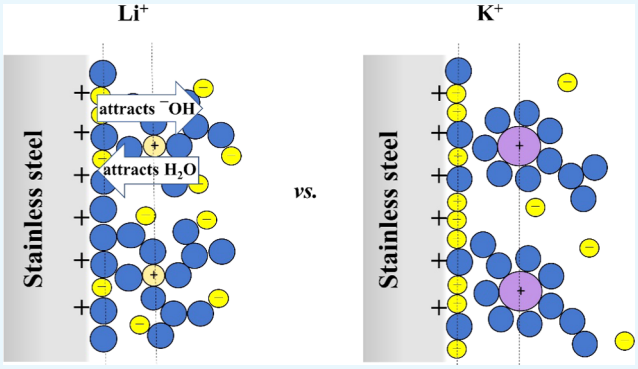

1. INTRODUCTION AND BACKGROUND

Corrosion-induced degradation of core-internal components composed of austenitic stainless steel in nuclear power plants often originates from localized (pitting) corrosion and intergranular stress corrosion cracking.[1] The primary factors that contribute to corrosion activity include: (1) exposure to halide ions (e.g., Cl^-, F^-) borne in the cooling water, (2) irradiation-induced alterations of the microstructure of stainless steel,[2,3] and (3) cooling water chemistry (e.g., pH, amounts of dissolved oxygen, and composition of cooling water additives) all of which can act to enhance or inhibit corrosion rates.[4]

Most often, studies of alloy corrosion have focused on Cl^- species due to their well-known role in accelerating the decomposition of the passivating oxide film, and thereby initiating corrosion.[5−13] Three models have been proposed for oxide layer breakdown in the presence of halides, namely,[7] (1) the adsorption model,[8,9] in which adsorbed halides form a metal cation complex within the oxide layer, which accelerates film removal, (2) the penetration model,[10,11] in which the penetration of halides results in the formation of conductive pathways within the oxide film that facilitate the transfer of metal cations from the surface into the bulk, and (3) the film breakdown model,[12,13] which suggests that the presence of adsorbed halides decreases the surface tension of the oxide, resulting in its mechanical rupture. These mechanisms are, however, applicable for systems involving a halide ion and a well-oxidized substrate. However, finer-scale understanding of the role of the accompanying (counter) cation on oxide film formation, growth, and stability remain less understood.

In nuclear power plants, lithium hydroxide (LiOH) is often used as a coolant additive to facilitate alkalinization (pH =

Received: August 30, 2018
Accepted: October 22, 2018
Published: November 1, 2018

DOI: 10.1021/acsomega.8b02227
ACS Omega 2018, 3, 14680−14688

6.9−7.4)[4] and thereby retard alloy corrosion at subcritical conditions.[4,14−19] However, under the operational conditions expected to be employed in the next generation of reactors, wherein temperature and pressure are within the critical limit, decreases in water density have been observed.[4,20] This results in a continuous increase in ionic association between Li^+ and ^-OH ions, making pH control difficult, thereby promoting oxide breakdown and accelerating corrosion.[4,14,21] Moreover, the concentration of Li^+ ions in crevices, leading to stress corrosion cracking of irradiated austenitic stainless steel in pressurized water reactors, has also been reported.[22] These issues highlight a need to better examine alternative alkali hydroxides that will facilitate better pH control, as opposed to LiOH, in nuclear reactors. Of particular interest is KOH because the K^+ ion has a smaller charge density compared to Li^+[22] and therefore, it exhibits a lower affinity for the negatively charged ^-OH ion,[24,25] making water chemistry control more manageable. Moreover, KOH is substantially (at least 5 times)[26] cheaper than LiOH and can be sourced much more readily than nuclear-grade[7] Li-hydroxide. As such, the use of KOH as compared to LiOH would result in substantial reductions in plant operational costs.

Herein, a combination of scanning electrochemical microscopy (SECM) and atomic force microscopy (AFM) is used to examine the impact of Li^+ and K^+ ions, for the first time, on the surface reactivity of passivated 304L stainless steel. The results offer new understanding of the role of (counter) cations, such as Li^+ and K^+, in inhibiting or otherwise affecting surface reactivities, an issue, which is of relevance to applications ranging from cooling water chemistry and steel corrosion, to batteries and other electrochemical devices.

2. RESULTS AND DISCUSSION

2.1. Effects of Alkali Cations on the Electrical Double Layer and Interaction Forces. Attractive and repulsive forces of interaction within a few nanometers away from a surface (e.g., van der Waals, electrostatic, hydration), e.g., in the region of the electrical double layer (EDL) can be estimated from the approach curve as the silicon nitride lever (SNL) probe approaches the steel surface.[27] Figure 1 shows that the approach force−distance curve in KOH more closely resembles that in deionized (DI) water as compared to LiOH, albeit with a positive minimum value, indicating attraction of the silicon nitride probe toward the substrate within 8 nm of separation distance in DI water. This behavior in DI water (measured pH = 5.8 at around 23 °C) is attributed to the attractive force between the negatively charged silicon nitride tip at the relevant solution pH[28] and the unpassivated (although oxidized) stainless steel surface, which exhibits a positive surface charge at pH ≤ 7.8.[48] The partial tip−substrate attraction observed in 10 mM KOH solutions at tip−substrate separation distances of ≤5 nm is due to the interaction of the negatively charged silicon nitride tip with the weakly hydrated K^+ ions and is much less pronounced compared with that observed in DI water because the increase in ion concentration results in a decrease in the length scale dominated by electrostatic attraction (i.e., due to compaction of the EDL).[29]

Furthermore, the approach curve featured a region at separations beyond 5 nm in which repulsive forces between the substrate and the tip are indicated. This repulsion of the SNL probe at distances >5 nm is indicative of hydration forces[27] and may also reflect the abundance of hydroxide (^-OH) ions on the steel surface, which is expected in alkaline conditions

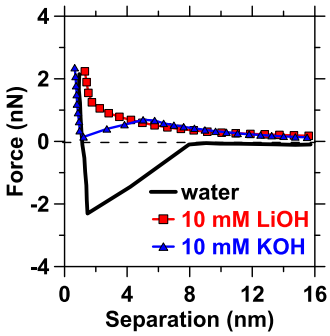

Figure 1. Representative force−distance (approach) curves of a 304L stainless steel substrate interacting with a silicon nitride lever (SNL-C) probe (tip diameter ≈ 12 nm) at 23 ± 3 °C in DI water, 10 mM KOH, and 10 mM LiOH solutions. The calculated Debye length (λ_D) in the 10 mM solutions is around 3 nm. In water, attraction between the negatively charged AFM tip and the positively charged steel surface occurs within separation distances of ≤8 nm. In KOH, both attraction and repulsion act on the AFM tip at separation distances of ≤5 nm. However, at surface separations >5 nm, repulsive forces are dominant due to both hydration forces and the abundance of ^-OH ions on steel surfaces. In LiOH, repulsive forces dominate both within and beyond 5 nm from the surface. This greater degree of repulsion of the AFM probe is consistent with the higher energy barrier to nanoscale structures[30] presented by the layer of hydrated Li^+ ions at the (steel−solution) interface.

(≥pH 10).[48] At lower ionic concentrations (i.e., 10 mM), repulsive forces are typically attributed to hydration instead of steric forces.[29] On the other hand, the interaction between the SNL probe and the substrate in LiOH solutions both within and beyond 5 nm from the steel is dominated by repulsive forces. The observed repulsion of the negatively charged SNL probe upon approach suggests that the steel surface becomes increasingly negatively charged in LiOH solutions, e.g., due to the presence of ^-OH ions contained within the hydration sphere of Li^+. This greater degree of repulsion identified by the SNL probe in LiOH solutions is consistent with the higher energy barrier to nanoscale structures[30] resulting from the layer of hydrated Li^+ ions that are present at the substrate−solution interface.[27,30]

Small ions with high charge density, like Li^+, are commonly referred to as kosmotropes (structure makers), whereas ions having lower charge densities, such as K^+, are chaotropes (structure breakers), e.g., see Figure 2.[23,31] Li^+ features a greater hydration energy (−515 kJ) compared to K^+ (−312 kJ),[32] thus forming a larger hydration sphere in water.[23] Kosmotropes are attracted to hydrophilic surfaces and repelled from hydrophobic ones.[23,33] On the other hand, chaotropes are relatively more attracted to hydrophobic surfaces following the solubility rule that "like dissolves like".[23,31] This suggests that hydrated Li^+ ions exhibit a stronger ion−surface interaction with the hydrophilic steel surface, resulting in ion adsorption and disruption of the EDL, a region consisting of two oppositely charged layers at the interface of two different phases in solution,[33] that persists on the surface of the steel. Figure 3 shows that the first layer of the EDL on stainless steel is composed of the following: a positively charged surface due to the work function difference between the steel and the solution;[43] the Stern layer (∼1 nm thickness),[34] which consists of the inner Helmholtz plane (composed of counterions, e.g., ^-OH ions in alkaline solutions, and solvent molecules, e.g., water); outer Helmholtz plane (composed of hydrated cations

DOI: 10.1021/acsomega.8b02227
ACS Omega 2018, 3, 14680−14688

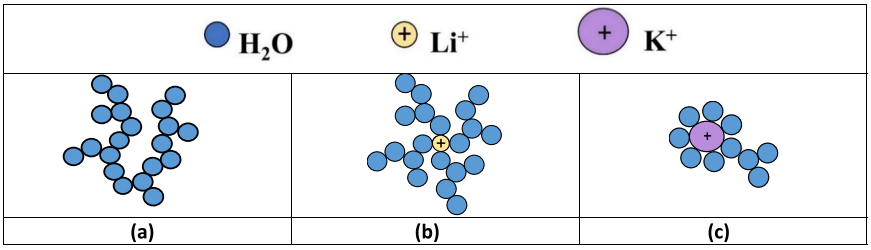

Figure 2. Representative illustrations of structures of: (a) bulk water, (b) strongly hydrated 4-coordinate Li^+ ions (kosmotrope), and (c) weakly hydrated 7-coordinate K^+ ion (chaotrope). This illustration is representative only and not drawn to scale.

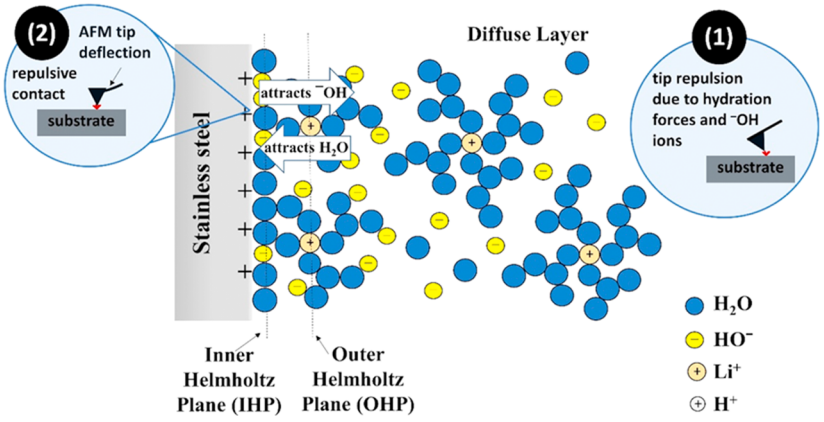

Figure 3. Illustration of the structure of the electrical double layer (EDL) that forms on an (oxidized) steel surface in LiOH solutions. The dehydration of Li^+ ions results in the sorption of ^-OH species from the steel substrate and from adsorbed H_2O molecules. These actions lead to: surface dealkalization (i.e., due to enrichment of H^+ ions at the steel−solution interface) and transport of the liberated (dissolved) Fe-species into the bulk solution. The resulting force−distance curves can be explained as follows: (1) the repulsion of the negatively charged silicon nitride tip within a few nanometers from the steel surface occurs due to the strong hydration forces surrounding the Li^+ ions and an abundance of ^-OH ions, which shield the positively charged metal surface. (2) When the AFM probe touches the surface of the steel substrate, a repulsive contact force is observed due to the overlapping molecular orbitals of the tip and substrate.[27] Therefore, (1) and (2) result in an overall (net) state of repulsive interaction.

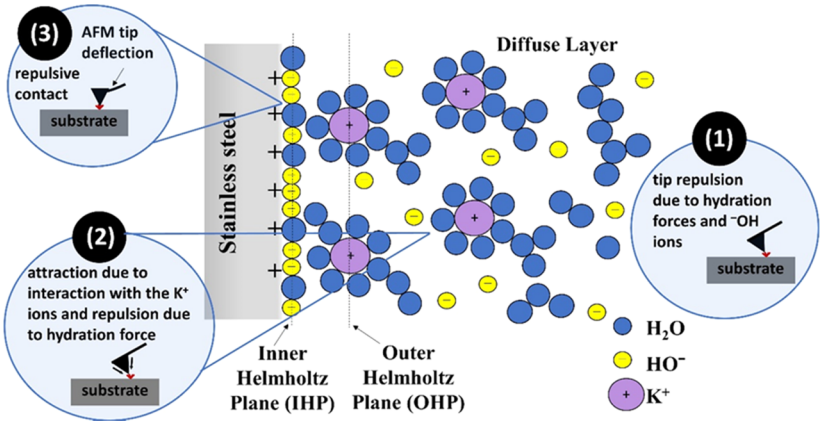

Figure 4. Illustration of the structure of the electrical double layer (EDL) that forms on an (oxidized) steel surface in KOH solutions. The force−distance curves can be explained as follows: (1) repulsion of the silicon nitride probe is observed at tip−substrate separation distances >5 nm due to hydration forces presented by the hydrated K^+ ions. These hydration forces are, however, weaker than those observed in hydrated Li^+ ions. (2) Both attractive and repulsive forces act on the negatively charged SNL probe at distances of ≤5 nm from the steel surface because of interactions with the weakly hydrated, positively charged K^+ ions, and van der Waals forces. (3) When the tip of the AFM probe touches the substrate, a repulsive force is observed.

attracted toward the surface); and the diffuse layer (where ions and molecules feature higher mobility).[33] Partial dehydration of the strongly hydrated Li^+ ions is suggested to occur on the water-deficient steel surface although the first hydration sphere is retained.[31] It is postulated that the dehydrated Li^+ ions will acquire ^-OH ions (displaced from the Stern layer[35,36] after surface dehydration of Li^+ ions) from the steel surface and water molecules present in the EDL. These actions induced by the presence of Li^+ result in the disruption of the EDL, and local dealkalization of the steel substrate resulting in the accelerated and enhanced interactions between the substrate and the aqueous species viz-a-viz when K^+ species are present,

DOI: 10.1021/acsomega.8b02227
ACS Omega 2018, 3, 14680−14688

e.g., which may result in an enhanced breakdown of the oxide film and Fe transport into solution over extended time scales.

Similar to Li^+ species, hydrated K^+ ions also undergo changes in their hydration sphere as they come into contact with the steel surface. However, unlike Li^+, the ion−surface interaction between the hydrophilic substrate and a chaotrope like hydrated K^+ ion is much weaker. Therefore, although hydrated K^+ ions will be incorporated into the EDL, this action does not lead to a significant disruption of the EDL (see Figure 4). For example, since it is known that the corrosion of stainless steel does not readily occur in pure water due to the presence of an oxide film,[33] it appears as though a lesser extent of disruption of the EDL, as apparent in KOH solutions as compared to LiOH solutions, signifies a condition that is suitable for the formation and maintenance of a more compact EDL and a less reactive (more oxidized) surface.

The collective of approach curves shown in Figure 1 were fitted using the Derjaguin−Landau−Verwey−Overbeek (DLVO) approximation to estimate the surface potential/charge of stainless steel in LiOH and KOH solutions. Two boundary conditions were used to fit the approach curves: constant-potential (CP) and constant-charge (CC). In the CP model, the surface potentials of the two opposing surfaces are assumed to remain constant as they approach each other. On the other hand, the surface charge densities of the opposing surfaces remain constant in the CC model.[31] In this study, the values of the parameters (surface charge densities and surface potentials of the AFM tip and substrate) were varied until best fits to eqs 1 and 2 representing CC and CP boundary conditions, respectively, were achieved. Both models, however, have the tendency to deviate from experimental results especially at separation distances less than 5 nm such that an underestimation of the observed force occurs, particularly when van der Waals interactions are considered.[37] This deviation has been attributed to the additional repulsive force introduced by solvent ordering (hydration layers) at the interface.[32,37−40] This method of fitting resulted in the following parameters: (1) surface charge density of the sample: −0.35 C/m^2, (2) surface charge density of the SNL probe: −0.05 C/m^2, and (3) electrical surface potential of the SNL probe: −0.7 V. The estimated electric surface potentials (i.e., the φ_2)[44] of 304L stainless steel in 10 mM LiOH and KOH solutions were −0.21 ± 0.005 and −0.19 ± 0.003 V, respectively, indicating that the interaction between the stainless steel and SNL probe surfaces is better rationalized using the CP boundary conditions. It should be noted that the CP model provides a better approximation for conductive (metallic) surfaces.[46] Furthermore, the CP model accurately represents the behavior of the force curves when the surfaces of the tip and the substrate have potentials of the same sign (i.e., negative). For example, repulsive interactions are observed at large separations, which becomes attractive as the tip and substrate approach each other.[37] The more negative surface potential that was calculated for stainless steel in LiOH is consistent with the presence of higher amounts of negatively charged species (e.g., ^-OH) within the hydration sphere of Li^+, as compared to K^+, in the EDL. This outcome is also in agreement with literature reports wherein the surface potential of a negatively charged substrate (e.g., stainless steel) is noted to increase in magnitude (more negative) with increasing hydration radius of the electrosorbed cations (i.e., since hydration radius of Li^+ is larger than that of K^+).[34]

2.2. Electrochemical Behavior of Steel Surfaces in the Presence of Alkali Cations. To validate the hypothesis that surface oxidation is indeed inhibited by the presence of kosmotropes (hydrated Li^+ ions) and the associated disruption of the EDL, potentiodynamic polarization and SECM analyses were carried out. Anodic polarization of 304L stainless steel in 10 mM LiOH and KOH solutions resulted in well-defined Tafel regions, as shown in Figure 5. The resulting plots

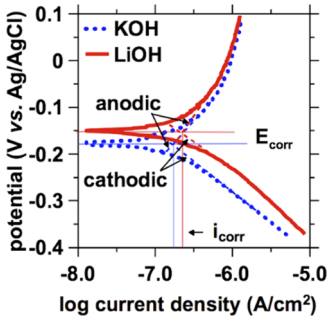

Figure 5. Representative Tafel plots generated via potentiodynamic polarization of 304L stainless steel in 10 mM LiOH (red curve) and 10 mM KOH (dotted blue curve) solutions. The corrosion potential (E_{corr}) and corrosion current density (i_{corr}) were determined from the intersection of the extrapolated anodic and cathodic segments, which are shown by the dashed blue and red lines, respectively.

revealed that the calculated corrosion current density (i_{corr}) under immersion in 10 mM LiOH is 2.03 × 10^{-7} A/cm^2, which is slightly higher than that in 10 mM KOH (i_{corr} = 1.55 × 10^{-7} A/cm^2). First, this identifies that acceleration of the electrode−solution interaction rates occurs in the presence of Li^+. Second, the calculated corrosion potentials (E_{corr}) in the LiOH and KOH solutions were identified as −0.15 ± 0.005 and −0.18 ± 0.002 V (vs Ag/AgCl), respectively. The lower E_{corr} value in KOH suggests a slower cathodic reaction (oxygen reduction),[41] indicating the presence of a compact EDL (and potentially, a better oxidized surface), is promoted in solutions containing hydrated K^+ ions as compared to those containing hydrated Li^+ species. On the other hand, identical anodic behaviors were observed between the Li- and K-containing solutions indicating similar anodic passivation processes. Note that E_{corr} refers to the mixed potential that is dependent on both the anodic and cathodic reactions[42] and is distinct from the surface potential of the substrate determined using DLVO analysis. Although the observed differences in the Tafel polarization curves suggest that surface reactivity and consequently the kinetics of cathodic reactions are indeed influenced by the EDL, a definite conclusion regarding the effect of cations cannot be derived due to the small difference between i_{corr} and E_{corr} assessed in relevant solutions. Therefore, to acquire better evidence on the effect of alkali cations on the oxidation of stainless steel, SECM studies were carried out both in the presence and absence of applied potential.

Figure 6 shows the results of SECM experiments carried out at open circuit potential (OCP) in feedback mode, with 1 mM FcMeOH as the redox mediator in 100 mM solutions of KOH and LiOH. The use of a redox mediator allowed for the analysis of how the formation of an oxide layer may screen the (initially) conductive steel surface. For example, a lower tip current should be observed in the presence of a less reactive surface because of the inhibited regeneration of the redox mediator (reduction of Fc^+) on the substrate. Interestingly,

DOI: 10.1021/acsomega.8b02227
ACS Omega 2018, 3, 14680−14688

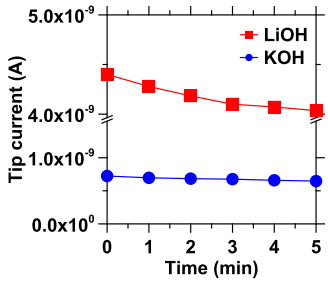

Figure 6. Evolution of the tip current measured using a 10 μm Pt ultramicroelectrode on the surface of 304L stainless steel immersed in 100 mM hydroxide solutions. The initial (and terminal, i.e., t = 75 min) currents measured in LiOH solutions are substantially higher than in KOH solutions, suggesting that a more inert surface persists in the latter case.

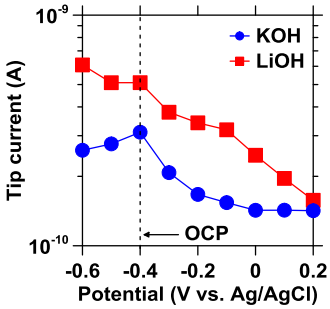

Figure 7. Representative plot of the tip current as a function of the applied potential. The open circuit potential (OCP) is represented by the dashed line. Herein, potentials were applied in the following order: (1) OCP (−0.4 V), (2) −0.3 V, (3) −0.5 V, (4) −0.2 V, (5) −0.6 V, (6) −0.1 V, (7) 0 V, (8) 0.1 V, (9) 0.2 V. Each applied potential was held for 5 min or until the rate of change in the tip current as a function of time (dI/dt) was less than 1.0×10^{-11} A/min indicating near-equilibrium conditions. It is seen that in the presence of increasingly positive applied potentials, the tip current exponentially decayed to a limiting value in KOH, suggesting inhibited surface reaction kinetics.

Figure 6 shows dramatic differences in the initial currents observed in solutions of LiOH (4.5×10^{-9} A) and KOH (0.7×10^{-9} A), e.g., due to the rapid surface oxidation of the steel surface in KOH solutions. Indeed, a decrease in current from ~2.0×10^{-9} to ~1.0×10^{-9} A was detected simply as the tip approached the surface (over a period of seconds) consistent with the rapid formation of an oxide film on stainless steel. It is therefore clarified that the higher tip current measured in the presence of Li^+ supports the premise that kosmotropes, such as hydrated Li^+ ions, perturb the electric double layer resulting in a more cathodically charged surface (e.g., see Figure 1). It should moreover be noted that even following extended exposure, i.e., after 75 min, the tip current in the presence of 100 mM LiOH (3.5×10^{-9} A) remained nearly 6.5 times higher as compared to an isoconcentration solution of KOH (5.5×10^{-10} A). The evolution of the tip current in both cases suggests the time-dependent growth and thickening of the oxide layer.

Next, the steel surface was polarized to assess whether kosmotropes may exhibit stronger ion−surface interaction with the substrate as opposed to chaotropes. The application of a bias was used to evaluate ion adsorption with applied potentials in the presence of Li^+ and K^+. This is based on the premise that in the presence of a positive potential, facilitated electrosorption of ^-OH on the substrate should be favored. Therefore, a corresponding current decrease should be observed similar to what has been observed at open circuit potential. On the other hand, the application of a negative potential should lead to the repulsion of ^-OH and attraction of the alkali cations toward the substrate and also result in the enhanced reduction of the redox mediator (FcMeOH). The change in tip current with respect of the applied potential offers insight into the strength of ion−surface interaction. For example, if hydrated Li^+ sorbs on the surface more strongly than hydrated K^+, a higher anodic potential would be needed in LiOH solutions because of the greater driving force needed to remove the strongly adsorbed hydrated Li^+ ions from the surface before the adsorption of ^-OH ions can occur.

The OCP measured in both LiOH and KOH solutions following 10 min of immersion was around ~−0.4 V vs Ag/AgCl. As shown in Figure 7, polarization to more positive regions of static potential ($E \geq -0.4$ V) resulted in a decrease in tip current consistent with the inhibited reduction of FcMeOH at the surface. It should be noted that independent of the application of potentials that are either more positive or more negative compared to the OCP, the tip current plateaued faster in KOH than in LiOH solutions. This supports the observations in Figure 6, i.e., the rate of oxide formation is faster in KOH solutions even in the presence of an applied bias. Further, a much lower potential was needed in KOH (0 V) than in LiOH (0.2 V) to facilitate a decrease to a limiting current of ~1.2×10^{-10} A. This suggests inhibited surface reactivity in the presence of KOH because hydrated K^+ ions exhibit a weaker interaction with the surface and therefore perturb the EDL to a much lesser degree, compared to hydrated Li^+ ions. Taken together, these SECM results support the premise of the AFM force spectroscopy studies and validate our hypothesis that hydrated Li^+ ions (kosmotropes) interrupt the EDL, and compete with ^-OH ions for adsorption at the surface of the substrate, resulting in enhanced surface reactivity of the stainless steel when such cations may be present.[a]

3. SUMMARY AND CONCLUSIONS

The influence of Li^+ and K^+ species on the surface reactivity of 304L stainless steel was investigated using a pioneering combination of scanning electrochemical microscopy (SECM) and atomic force microscopy (AFM)-based force spectroscopy analysis. Critical analysis of the force curves was used to reveal fine-scale insights into interactions of the hydrated alkali cations with the passivated stainless steel surface. Specifically, repulsion of the negatively charged silicon nitride probe was observed as it approached the substrate in the presence of both hydrated Li^+ and K^+ ions. However, attractive forces emerged within 5 nm of the surface in KOH solutions, but not in LiOH solutions. These observations offer evidence of the greater extent of shielding of the positively charged substrate due to ion−surface interaction between the hydrophilic stainless steel and the hydrated Li^+ ions (kosmotrope), as compared to that with hydrated K^+ ions (chaotrope). Analysis of the force curves within the framework offered by the DLVO approximation revealed that the surface potential of stainless steel in LiOH was more negative than in KOH, consistent with the dominance of repulsive forces observed in the former case. These observations arise because as hydrated Li^+ ions adsorb on the surface of stainless steel,

DOI: 10.1021/acsomega.8b02227
ACS Omega 2018, 3, 14680−14688

they dehydrate (i.e., forego solvated water). To ensure charge compensation, the dehydrated Li^+ ions preferentially adsorb ^-OH from H_2O molecules sited on the surface and within the EDL thereby resulting in the disruption of the EDL. This concept was validated by SECM analyses, which confirmed that the ability of the steel surface in LiOH solutions to promote redox reactions is indeed higher as compared to that in KOH solutions, as evidenced by the higher currents of FcMeOH measured both at open circuit and in the presence of an applied potential. The outcomes provide direct evidence regarding the potentially detrimental effects of Li^+ on stainless steel by facilitating surface reactions (e.g., corrosion), which therefore warrants further studies of water chemistry control in conditions of relevance to nuclear power plants (e.g., with irradiation exposure under superheated conditions). On a broader level, these findings provide critical insights regarding cation−surface interactions beyond corrosion, as relevant to applications including the development of high-performing, durable electrodes, which may find use in batteries and electrocatalysts.

4. MATERIALS AND METHODS

Reagent grade lithium hydroxide (LiOH; Fisher Scientific, anhydrous), potassium hydroxide (KOH; Fisher Scientific, 88.5%), and ferrocenemethanol (FcMeOH; $C_{11}H_{12}FeO$; Alfa Aesar, 97%) were used. Deionized (DI) water was obtained from a Millipore Milli-Q Integral water purification system (>18 MΩ cm).

Commercially available 304L stainless steel (McMaster-Carr) was sectioned into coupons having dimensions of 1.2 cm × 0.8 cm × 0.3 cm (length × width × height) using a low-speed precision saw (Buehler, IsoMet 1000). The nominal composition (in mass %) of the steel, as provided by the supplier is Fe (70.89%), C (0.016%), Mn (1.77%), P (0.029%), S (0.001%), Si (0.26%), Cr (18.18%), Ni (8.02%), Mo (0.35%), Cu (0.39%), and N (0.090%). The solution-annealed steel samples (with an average grain size of around 40 μm) were embedded in epoxy resin, which was allowed to cure overnight at room temperature. The samples were then polished using 400-, 600-, 800-, and 1200-grit sandpaper, followed by 3 and 1 μm diamond pastes and finally with 0.05 μm colloidal silica suspension until they featured a surface roughness on the order of S_z = 2 nm. In general, the samples were rinsed with DI water and then with ethanol prior to switching to the next polishing material to minimize contamination. This step was followed by ultrasonication in acetone and in isopropanol, each for 30 s, and drying with a stream of ultrahigh purity nitrogen gas.

4.1. Atomic Force Microscopy (AFM). Force spectroscopy was carried out in contact mode using a Bruker FastScan AFM to investigate the perturbation of the electrical double layer (EDL) caused by hydrated Li^+ and K^+ ions present on the steel surface. Special focus was paid to monitor the attractive and repulsive forces of interaction (i.e., between the substrate and the AFM tip in the presence of electrosorbed ions and the bulk solution) that are inferred from the deflection of the cantilever as a function of tip−substrate separation. As such, force spectroscopy was carried out, in solution, on 304L stainless steel coupons that were immersed in DI water or 10 mM solutions of LiOH or KOH.

A silicon nitride lever (Bruker, SNL-C) probe with a silicon nitride tip diameter of 12 nm (i.e., estimated using scanning electron microscopy) was used. Surface mapping was carried out in contact mode in deionized water wherein nine different locations, well-separated from each other, were selected for force spectroscopy measurements. The interaction forces were measured by bringing the SNL-C probe into contact with the substrate. Fifty ramps were performed at each point (450 ramps per run) using a ramp size of 500 nm and a tip velocity of 420 nm/s. The surface of the substrate was rigorously flushed with DI water, and force−distance curves were acquired (i.e., to ensure that the flushed surface's response matched that of a pristine surface in contact with DI water) before switching to another metal hydroxide solution. The force curves were processed using the Bruker NanoScope Analysis software (v.1.8) to convert the curves from deflection−height diagrams to force−separation (F−D) diagrams using the deflection sensitivity (137.7 nm/V) and spring constant (0.3839 N/m) measured under immersion. All AFM measurements were performed at 23 ± 2 °C.

The interaction forces between the tip and the steel surface can be analyzed within the framework of the Derjaguin, Landau, Verwey, and Overbeek (DLVO) theory, which predicts the net interaction between two charged surfaces and provides an estimate of the forces of interaction. The forces herein include a combination of van der Waals and electrostatic (i.e., due to double layer contributions) at various separation distances between two surfaces.[45] To provide an approximation of the forces of interaction between the conical tip and the planar substrate, the force−distance curves were fitted using models for constant-charge (CC) and the constant-potential (CP) boundary conditions, respectively.[46,47] The CC (eq 1) and CP (eq 2) equations are expressed as follows[46]

$$F_{\mathrm{DLVO}}^{\mathrm{CC}} = \frac{2\pi R\lambda_{\mathrm{D}}}{\varepsilon\varepsilon_0}[2\sigma_{\mathrm{S}}\sigma_{\mathrm{T}}\, \mathrm{e}^{-D/\lambda_{\mathrm{D}}} + (\sigma_{\mathrm{S}}^2 + \sigma_{\mathrm{T}}^2)\, \mathrm{e}^{-2D/\lambda_{\mathrm{D}}}] - \frac{AR}{6D^2} \quad (1)$$

$$F_{\mathrm{DLVO}}^{\mathrm{CP}} = \frac{2\pi R\lambda_{\mathrm{D}}}{\varepsilon\varepsilon_0}[2\psi_{\mathrm{S}}\psi_{\mathrm{T}}\, \mathrm{e}^{-D/\lambda_{\mathrm{D}}} - (\psi_{\mathrm{S}}^2 + \psi_{\mathrm{T}}^2)\, \mathrm{e}^{-2D/\lambda_{\mathrm{D}}}] - \frac{AR}{6D^2} \quad (2)$$

where D is the separation distance between the tip and the substrate (in nm); R is the tip radius (in nm); σ_{T} and σ_{S} are the surface charge densities of the AFM probe and substrate (in C/m^2), respectively; ψ_{T} and ψ_{S} are the surface potentials of the AFM probe and substrate (in V), respectively; ε is the dielectric constant of the medium (78.54 for an aqueous electrolyte solution);[46] ε_0 is the permittivity of vacuum (8.854×10^{-12} F/m); A is the Hamaker constant (2.88×10^{-19} J);[48] and λ_{D} is the Debye length (3 nm for 10 mM 1:1 symmetric electrolyte containing LiOH and KOH as estimated from the ionic strength[46]). It should be noted that the DLVO fitting is only valid at distances greater than around 6 nm because of hydration forces and the finite size of ions.[49] Therefore, fits were performed over separation distances of 7−70 nm from the surface.

4.2. Potentiodynamic Polarization. Anodic polarization of stainless steel coupons was carried out in 10 mM solutions of LiOH and KOH using a HEKA PG-618 potentiostat. A Ag/AgCl electrode and a Pt (platinum) wire were used as reference and counter electrodes, respectively. The potential was linearly swept from −0.4 to +0.2 V (vs Ag/AgCl) at a scan rate of 0.17 V/s. The corresponding Tafel plots were generated

DOI: 10.1021/acsomega.8b02227
ACS Omega 2018, 3, 14680−14688

by plotting the applied potential versus the logarithm of the current density. From these plots, the corrosion potential (E_{corr}) and corrosion current density (i_{corr}) were determined using the points of intersection of the extrapolated linear cathodic and anodic Tafel segments. All experiments were performed at 23 ± 3 °C.[b]

4.3. Scanning Electrochemical Microscopy (SECM). The effects of Li^+ and K^+ ions on the formation, stability, and decomposition of the oxide film were evaluated using a HEKA ElProScan SECM in feedback mode, using 1 mM ferrocenemethanol (FcMeOH, $C_{11}H_{12}FeO$) as the redox mediator. The background solutions used consisted of 100 mM KOH and LiOH. The use of alkali hydroxides instead of chloride solutions ensured that halide-induced effects (e.g., inhibition of oxide formation and degradation of the passive film) will not occur and that any observed difference in the behavior of the overlayer can be attributed directly to the alkali cation of interest. It should be noted that although the concentrations used herein (100 mM) are higher than that used in nuclear plants, this selection was made to induce measurable changes, expediently, at ambient temperature.

The reference electrode used was Ag/AgCl, and the counter electrode consisted of a Pt wire. A potential of +0.4 V vs Ag/AgCl was applied to oxidize ferrocene ($C_{10}H_{10}Fe$) to the ferrocenium ion ($[C_{10}H_{10}Fe]^+$) at the tip of the Pt ultramicroelectrode (Pt UME). In this setup, the ferrocenium ion produced at the UME tip is reduced back to ferrocene at the surface of a conductive substrate. This continuous regeneration of the redox mediator results in an increasing tip current as the electrode approaches a reactive surface. On the other hand, a decrease in tip current is observed in the proximity of inert substrates due to reduced regeneration and diffusion of the redox mediator to the Pt UME tip.[51]

The SECM when operated in constant distance mode allows for the interpretation of electrochemical signals independent from local topography by controlling the tip-to-substrate separation using the feedback response.[52−54] The basis of such measurements is as follows. The application of an alternating potential to the diether (stimulation) piezo results in the oscillation of the UME. As the UME tip approaches the surface of the substrate, shear force damping is observed resulting in amplitude and phase (frequency) shifts of the oscillation of receiver piezo.[55] The amplitude (in mV) and frequency (in kHz) set points can be determined by comparing the frequency spectra collected on the surface of the substrate and in bulk solution (i.e., ≥10 μm above the surface). The frequency used herein was 365 kHz and the amplitude set point was 10 mV, which was 10% of the change in amplitude when the UME was retracted by 3 μm from the surface of the substrate. Following so, the tip current of the 10 μm Pt UME as it contacts the 304L stainless steel surface was measured. All experiments were performed at 23 ± 3 °C.

AUTHOR INFORMATION

Corresponding Author

*E-mail: gsant@ucla.edu. Phone: (310) 206-3084.

ORCID

Erika Callagon La Plante: 0000-0002-5273-9523

Gaurav Sant: 0000-0002-1124-5498

Notes

The authors declare no competing financial interest.

ACKNOWLEDGMENTS

The authors acknowledge financial support for this research provided by the U.S. Department of Energy's Light Water Reactor Sustainability (LWRS) Program through the Oak Ridge National Laboratory operated by UT-Battelle LLC (Contract #: 4000154999) and The National Science Foundation (CAREER Award: 1253269). The contents of this paper reflect the views and opinions of the authors, who are responsible for the accuracy of data presented. This research was carried out in the Laboratory for the Chemistry of Construction Materials (LC^2) and the California Nanosystems Institute at UCLA. As such, the authors gratefully acknowledge the support that has made these facilities and their operations possible.

ADDITIONAL NOTES

[a]Contrastingly, analysis of the 304L stainless steel surfaces using electrical impedance spectroscopy and equivalent circuit modeling indicated very similar characteristics of the oxidized steel surface in the presence of both LiOH and KOH solutions. This may indicate a need for spatially localized, as opposed to bulk analysis of reacting surfaces to better elucidate the effects of solvent chemistry on surface reactivity.

[b]It should be noted that although these studies were carried at ambient temperatures, they offer a reliable model for systems at high(er) temperatures because the ionic association between Li^+ and ^-OH remains substantially higher than that between K^+ and ^-OH even at room temperature.[50]

REFERENCES

(1) Bruemmer, S. M.; Was, G. S. Microstructural and Microchemical Mechanisms Controlling Intergranular Stress Corrosion Cracking in Light-Water-Reactor Systems. *J. Nucl. Mater.* **1994**, *216*, 348−363.

(2) Nishioka, H.; Fukuya, K.; Fujji, K.; Kitsunai, Y. Deformation Structure in Highly Irradiated Stainless Steels. *J. Nucl. Sci. Technol.* **2008**, *45*, 274−287.

(3) McMurtrey, M. D.; Was, G. S.; Cui, B.; Robertson, I.; Smith, L.; Farkas, D. Strain Localization at Dislocation Channel−Grain Boundary Intersections in Irradiated Stainless Steel. *Int. J. Plast.* **2014**, *56*, 219−231.

(4) Carvajal-Ortiz, R. A.; Plugatyr, A.; Svishchev, I. M. On the pH Control at Supercritical Water-Cooled Reactor Operating Conditions. *Nucl. Eng. Des.* **2012**, *248*, 340−342.

(5) Sato, N. A Theory for Breakdown of Anodic Oxide Films on Metals. *Electrochim. Acta* **1971**, *16*, 1683−1692.

(6) Sato, N.; Kudo, K.; Noda, T. The Anodic Oxide Film on Iron in Neutral Solution. *Electrochim. Acta* **1971**, *16*, 1909−1921.

(7) Lee, J-S.; Kawano, T.; Ishii, T.; Kitagawa, Y.; Nakanishi, T.; Hasegawa, Y.; Fushimi, K. Initiation of Localized Corrosion of Ferritic Stainless Steels by Using the Liquid-Phase Ion Gun Technique. *J. Electrochem. Soc.* **2017**, *164*, C1−C7.

(8) Kolotyrkin, J. M. Pitting Corrosion in Metals. *Corrosion* **1963**, *19*, 261t−268t.

(9) Hoar, T. P.; Jacob, W. R. Breakdown of Passivity of Stainless Steel by Halide Ions. *Nature* **1967**, *216*, 1299−1301.

(10) Evans, U. R. The Passivity of Metals. Part I. The Isolation of the Protective Film. *J. Chem. Soc.* **1927**, 1020−1040.

(11) Hoar, T. P.; Mears, D. C.; Rothwell, G. P. R. The Relationships between Anodic Passivity, Brightening and Pitting. *Corros. Sci.* **1965**, *5*, 279−289.

(12) Hoar, T. P. The Production and Breakdown of the Passivity of Metals. *Corros. Sci.* **1967**, *7*, 341−355.

(13) Sato, N. A Theory of Breakdown of Anodic Oxide Films on Metals. *Electrochim. Acta* **1971**, *16*, 1683−1692.

DOI: 10.1021/acsomega.8b02227
ACS Omega 2018, 3, 14680−14688

(14) Svishchev, I. M.; Carvajal-Ortiz, R. A.; Choudhry, K. I.; Guzonas, D. A. Corrosion Behavior of Stainless Steel 316 in Sub- and Supercritical Aqueous Environments: Effect of LiOH Additions. *Corros. Sci.* **2013**, *72*, 20−25.
(15) Lister, D.; Uchida, S. Determining Water Chemistry Conditions in Nuclear Reactor Coolants. *J. Nucl. Sci. Technol.* **2015**, *52*, 451−466.
(16) Sawicki, J. A. Hydrothermal Synthesis of Ni_2FeBO_5 in Near-Supercritical PWR Coolant and Possible Effects of Neutron-Induced ^{10}B Fission in Fuel Crud. *J. Nucl. Mater.* **2011**, *415*, 179−188.
(17) Cox, B. Some Thoughts on the Mechanisms of In-Reactor Corrosion of Zirconium Alloys. *J. Nucl. Mater.* **2005**, *336*, 331−368.
(18) Pastina, B.; Isabey, J.; Hickel, B. The Influence of Water Chemistry on the Radiolysis of the Primary Coolant Water in Pressurized Water Reactors. *J. Nucl. Mater.* **1999**, *264*, 309−318.
(19) Bojinov, M.; Karastoyanov, V.; Kinnunen, P.; Saario, T. Influence of Water Chemistry on the Corrosion Mechanism of a Zirconium-Niobium Alloy in Simulated Light Water Reactor Coolant Conditions. *Corros. Sci.* **2010**, *52*, 54−67.
(20) Oka, Y.; Koshizuka, S.; Yamasaki, T. Direct Cycle Light Water Reactor Operating at Supercritical Pressure. *J. Nucl. Sci. Technol.* **1992**, *29*, 585−588.
(21) Plugatyr, A.; Carvajal-Ortiz, R. A.; Svishchev, I. M. Ion-Pair Association Constant for LiOH in Supercritical Water. *J. Chem. Eng. Data* **2011**, *56*, 3637−3642.
(22) Wang, M. I. Irradiated Assisted Corrosion of Stainless Steel in LWRs − Focus on Radiolysis and Corrosion Damage, 2013. https://hal.archives-ouvertes.fr/hal-00841142/document (accessed May 01, 2018).
(23) Mähler, J.; Persson, I. A Study of the Hydration of the Alkali Metal Ions in Aqueous Solutions. *Inorg. Chem.* **2012**, *51*, 425−438.
(24) Ho, P. C.; Palmer, D. A.; Wood, R. H. Conductivity Measurements of Dilute Aqueous LiOH, NaOH, and KOH Solutions to High Temperatures and Pressures Using a Flow-Through Cell. *J. Phys. Chem. B* **2000**, *104*, 12084−12089.
(25) Darken, L. S.; Meier, H. F. Conductances of Aqueous Solutions of the Hydroxides of Lithium, Sodium and Potassium at 25 °C. *J. Am. Chem. Soc.* **1942**, *64*, 621−623.
(26) ECVV. https://www.ecvv.com/ (accessed April 30, 2018).
(27) Leite, F. L.; Mattoso, L. H. C.; Olivieira, O. N.; Herrmann, P. S. P., Jr. The Atomic Force Spectroscopy as a Tool to Investigate Surface Forces: Basic Principles and Applications. In *Modern Research and Educational Topics in Microscopy*; Formatex, 2007; pp 747−757.
(28) Heinz, W. F.; Hoh, J. H. Relative Surface Charge Density Mapping with the Atomic Force Microscope. *Biophys. J.* **1999**, *76*, 528−538.
(29) Tsapikouni, T. S.; Allen, S.; Missirlis, Y. F. Measurement of Interaction Forces Between Fibrinogen Coated Probes and Mica Surface with the Atomic Force Microscope: The pH and Ionic Strength Effect. *Biointerphases* **2008**, *3*, 1−8.
(30) Fukuma, T.; Higgins, M. J.; Jarvis, S. P. Direct Imaging of Individual Intrinsic Hydration Layers on Lipid Bilayers at Angstrom Resolution. *Biophys. J.* **2007**, *92*, 3603−3609.
(31) Akpinar, E.; Turkmen, M.; Canioz, C.; Neto, A. M. F. Role of Kosmotrope-Chaotrope Interactions at Micelle Surfaces on the Stabilization of Lyotropic Nematic Phases. *Eur. Phys. J. E* **2016**, *36*, 107.
(32) Parker, J. L.; Christenson, H. K. J. Measurements of the forces between a metal surface and mica across liquids. *J. Chem. Phys* **1988**, *88*, 8013.
(33) Ishida, K.; Lister, D. In situ Measurement of Corrosion of Type 316 L Stainless Steel in 553 K Pure Water via the Electrical Resistance of a Thin Wire. *J. Nucl. Sci. Technol.* **2012**, *49*, 1078−1091.
(34) Brown, M. A.; Abbas, Z.; Kleibert, A.; Green, R. G.; Goel, A.; May, S.; Squires, T. M. Determination of Surface Potential and Electrical Double-Layer Structure at the Aqueous Electrolyte-Nanoparticle Interface. *Phys. Rev. X* **2016**, *6*, No. 011007.
(35) Vincent, B.; Bijsterbosch, B. H.; Lyklema, J. Competitive Adsorption of Ions and Neutral Molecules in the Stern Layer on Silver Iodide and Its Effect on Colloid Stability. *J. Colloid. Interface Sci.* **1971**, *37*, 171−178.
(36) Ostolska, I.; Wisniewska, M. Application of the Zeta Potential Measurements to Explanation of Colloidal Cr_2O_3 Stability Mechanism in the Presence of the Ionic Polyamino Acids. *Colloid Polym. Sci.* **2014**, *292*, 2453−2464.
(37) Hillier, A. C.; Kim, S.; Bard, A. J. Measurement of Double-Layer Forces at the Electrode/Electrolyte Interface Using the Atomic Force Microscope: Potential and Anion Dependent Interactions. *J. Phys. Chem.* **1996**, *100*, 18808−18817.
(38) Israelachvili, J. N.; Adams, G. E. Measurement of Forces between Two Mica Surfaces in Aqueous Electrolyte Solutions in the Range 0−100 nm. *J. Chem. Soc., Faraday Trans. 1* **1978**, *74*, 975−1001.
(39) Shubin, V.; Kekicheff, P. J. Electrical Double Layer Structure Revisited via a Surface Force Apparatus: Mica Interfaces in Lithium Nitrate Solutions. *J. Colloid Interface Sci.* **1993**, *155*, 108−123.
(40) O'Shea, S. J.; Welland, M. E.; Pethica, J. B. Atomic Force Microscopy of Local Compliance at Solid-Liquid Interfaces. *Chem. Phys. Lett.* **1994**, *223*, 336.
(41) Stephens, L. I.; Perry, S. C.; Gateman, S. M.; Lacasse, R.; Schulz, R.; Mauzeroll, J. Development of a Model for Experimental Data Treatment of Diffusion and Activation Limited Polarization Curves for Magnesium and Steel Alloys. *J. Electrochem. Soc.* **2017**, *164*, E3576−E3582.
(42) Tachibana, M.; Ishida, K.; Wada, Y.; Shimizu, R.; Ota, N.; Hara, N. Cathodic Polarization Curves of the Oxygen Reduction Reaction on Various Structural Materials of Boiling Water Reactors in High Temperature−High Purity Water. *J. Nucl. Sci. Technol.* **2012**, *49*, 551−561.
(43) Mott, N. F. "The theory of the formation of protective oxide films on metals.—III.". *Trans. Faraday Soc.* **1947**, *43*, 429−434.
(44) Bard, A. J.; Faulkner, L. R.; Leddy, J.; Zoski, C. G. *Electrochemical Methods: Fundamentals and Applications*; Wiley: New York, 1980; Vol. 2.
(45) Mikelonis, A. M.; Youn, S.; Lawler, D. F. DLVO Approximation Methods for Predicting the Attachment of Silver Nanoparticles to Ceramic Membranes. *Langmuir* **2016**, *32*, 1723−1731.
(46) Borghi, F.; Vyas, V.; Podesia, A.; Milani, P. Nanoscale Roughness and Morphology Affect the Isoelectric Point of Titania Surfaces. *PLoS One* **2013**, *8*, No. e68655.
(47) Butt, H.-J. Electrostatic Interaction in Scanning Probe Microscopy When Imaging in Electrolyte Solutions. *Nanotechnology* **1992**, *3*, 60−68.
(48) Song, Y. Y.; Bhadeshia, H. K. D. H.; Suh, D.-W. Stability of Stainless-Steel Nanoparticle and Water Mixtures. *Powder Technol.* **2015**, *272*, 34−44.
(49) Brant, J. A.; Childress, A. E. Membrane-Colloid Interactions: Comparison of Extended DLVO Predictions with AFM Force Measurements. *Environ. Eng. Sci.* **2002**, *19*, 413−427.
(50) Darken, L. S.; Meier, H. F. Conductances of Aqueous Solutions of the Hydroxides of Lithium, Sodium and Potassium at 25 °C. *J. Am. Chem. Soc.* **1942**, *64*, 621−623.
(51) Polcari, D.; Dauphin-Ducharme, P.; Mauzeroll, J. Scanning Electrochemical Microscopy: A Comprehensive Review of Experimental Parameters from 1989 to 2015. *Chem. Rev.* **2016**, *116*, 13234−13278.
(52) Eckhard, K.; Etienne, M.; Schulte, A.; Schuhmann, W. Constant-Distance Mode AC-SECM for the Visualization of Corrosion Pits. *Electrochem. Commun.* **2007**, *9*, 1793−1797.
(53) Ballesteros Katemann, B.; Schulte, A.; Schuhmann, W. Constant-Distance Mode Scanning Electrochemical Microscipy (SECM) Part I: Adaptation of a Non-Optical Shear-Force-Based Positioning Mode for SECM Tips. *Chem. - Eur. J.* **2003**, *9*, 2025−2033.
(54) Nebel, M.; Erichsen, T.; Schuhmann, W. Constant-Distance Mode SECM as a Tool to Visualize Local Electrocatalytic Activity of Oxygen Reduction Catalysts. *Beilstein J. Nanotechnol.* **2014**, *5*, 141−151.

DOI: 10.1021/acsomega.8b02227
ACS Omega 2018, 3, 14680−14688

(55) Dauphin-Ducharme, P.; Binns, W. J.; Snowden, M. E.; Shoesmith, D. W.; Mauzeroll, J. Determination of the Local Corrosion Rate of Magnesium Alloys Using a Shear Force Mounted Scanning Microcapillary Method. *Faraday Discuss.* **2015**, *180*, 331−345.

DOI: 10.1021/acsomega.8b02227
ACS Omega 2018, 3, 14680−14688